Title
Regulation of Organelle Acidity

Authors
Grabe, Michael
Oster, George

Regulation of Organelle Acidity[✪]

Michael Grabe* and George Oster[‡§]

From the *Department of Physics, ‡Department of Molecular and Cellular Biology, and §College of Natural Resources, University of California, Berkeley, Berkeley, California 94720

ABSTRACT   Intracellular organelles have characteristic pH ranges that are set and maintained by a balance between ion pumps, leaks, and internal ionic equilibria. Previously, a thermodynamic study by Rybak et al. (Rybak, S., F. Lanni, and R. Murphy. 1997. *Biophys. J.* 73:674–687) identified the key elements involved in pH regulation; however, recent experiments show that cellular compartments are not in thermodynamic equilibrium. We present here a nonequilibrium model of lumenal acidification based on the interplay of ion pumps and channels, the physical properties of the lumenal matrix, and the organelle geometry. The model successfully predicts experimentally measured steady-state and transient pH values and membrane potentials. We conclude that morphological differences among organelles are insufficient to explain the wide range of pHs present in the cell. Using sensitivity analysis, we quantified the influence of pH regulatory elements on the dynamics of acidification. We found that V-ATPase proton pump and proton leak densities are the two parameters that most strongly influence resting pH. Additionally, we modeled the pH response of the Golgi complex to varying external solutions, and our findings suggest that the membrane is permeable to more than one dominant counter ion. From this data, we determined a Golgi complex proton permeability of 8.1×10^{-6} cm/s. Furthermore, we analyzed the early-to-late transition in the endosomal pathway where Na,K-ATPases have been shown to limit acidification by an entire pH unit. Our model supports the role of the Na,K-ATPase in regulating endosomal pH by affecting the membrane potential. However, experimental data can only be reproduced by (1) positing the existence of a hypothetical voltage-gated chloride channel or (2) that newly formed vesicles have especially high potassium concentrations and small chloride conductance.

KEY WORDS: pH regulation • V-ATPase • proton leak • membrane potential

INTRODUCTION

Intracellular organelles have characteristic lumenal pHs suited to their biochemical function. Most of the organelles along the endocytic and secretory pathways, as well as lysosomes, maintain acidic interiors through the action of a primary electrogenic proton pump, the V-ATPase. From Fig. 1 A we see the diverse range of pHs present in the cell. It is our goal to understand the mechanisms that enable organelles to establish and maintain these lumenal pHs. In addressing this problem, we hope to elucidate the connection between organelle pH, morphology, and lumenal contents. We have constructed a model of acidification based upon specific membrane ion pumps and leaks and the internal ionic equilibria characteristic of the lumenal matrix material. Using the model, we have explored the mechanisms of acidification in specific organelles and deduced some general features of pH regulation.

Proton concentration plays a fundamental role in many cellular processes. These roles can be quite different. For instance, osteoclasts use low pH to dissolve bone, whereas neural synaptic vesicles utilize the pH gradient across the bilayer to drive the secondary transport of neurotransmitters (Moriyama and Futai, 1990; Chatterjee et al., 1992). Interestingly, organelles along both the secretory and endocytic pathways experience a gradient of decreasing pH (Cain et al., 1989; Fuchs et al., 1989; Wu et al., 2000). In endosomes, acidification is required for the proper sorting of receptors from ligands. An excellent review of these systems can be found in Futai et al. (2000).

Many of the pH regulatory elements appear in all cellular organelles. For instance, proton leaks have been identified in both the exocytic and secretory pathways, whereas V-ATPases appear to be integral components of nearly all organelles (Van Dyke and Belcher, 1994; Kim et al., 1996; Schapiro and Grinstein, 2000; Wu et al., 2000). Endosomes and Golgi complex are permeable to counter ions such as chloride and potassium, which can affect pH by altering the membrane potential (Van Dyke and Belcher, 1994; Schapiro and Grinstein, 2000). Although many regulatory elements are present in most, if not all, organelles, other elements appear to be restricted to particular organelles; e.g., the Na,K-ATPase that limits acidification in the early part of the endosomal pathway (Cain et al., 1989; Fuchs et al., 1989; Teter et al., 1998). Fig. 1 B lists the major el-
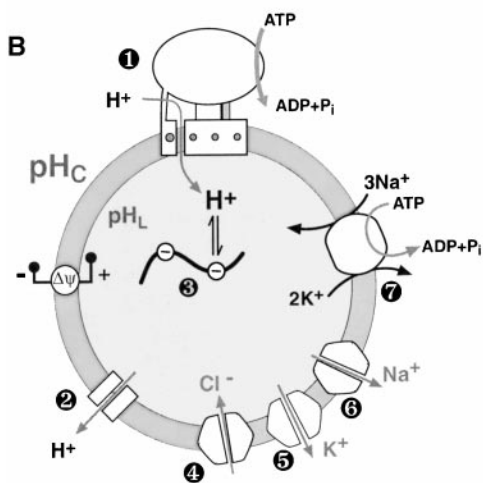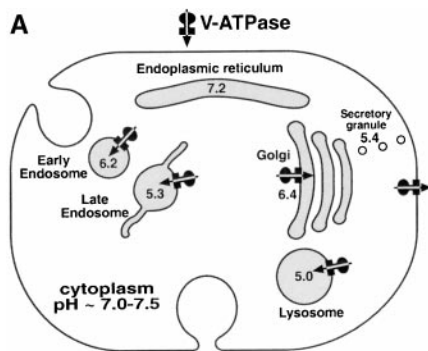

FIGURE 1.   (A) A prototypical mammalian cell showing the major organelles that exhibit distinct lumenal pHs along with typical pH values. These compartments tend to be in the secretory or endocytic pathways. Arrows indicate the progression along these pathways. (B) Cartoon of an organelle illustrating the principle elements influencing organelle pH regulation. (1) V-ATPase activity can be directly regulated, e.g., by dissociation of V_1; (2) passive proton leaks; (3) buffering by the lumenal polyelectrolyte matrix; (4) chloride channels; (5) potassium channels; (6) sodium channels; and (7) the Na,K-ATPase.

ements that we have considered in our study. Many of the seminal experiments from which this list was compiled will be discussed as we construct the model; for an alternative discussion see Rybak et al. (1997).

Motivation for our model comes from the large number of uncertainties and interrelated effects involved in pH regulation. It is often difficult to extract useful information from even the most precise experiments when the systems involved are as complex as the ones we have examined. Thus, a model based on the physics of membrane biology that employs realistic descriptions of the relevant bioenergetic proteins is useful in precisely interpreting experimental data. Since our model is kinetic, it is able to explain the entire pH curve measured during acidification experiments.

Thus, in addition to fitting steady-state data, our model can fit initial slopes and transients. From these fits, we determine the total numbers of pumps present in a particular experiment. In principle, using this analysis to compare different organelles can generate predictions about pump sorting events. While such biochemical information may be present in the experimental data, it requires a comprehensive model to quantify it. Sorting events, and hence their quantification, are critical to understanding pH regulation.

MATERIALS AND METHODS

A Model for Organelle Acidification

The problem of pH regulation largely reduces to regulating the activity of the vacuolar proton pumps (the V-ATPases), which are the primary acidifying agent for most cellular organelles. As an organelle acidifies, a proton motive force (pmf)[1] is built up that opposes further acidification. The transmembrane pmf ($\Delta\mu$) across an organelle bilayer has two components: (1) the membrane potential ($\Delta\psi$), and (2) the proton concentration gradient (ΔpH):

$$\text{pmf} \equiv \Delta\mu = \Delta\psi - 2.3\frac{k_B T}{e}\Delta pH, \tag{1}$$

where k_B is Boltzmann's constant, T is the absolute temperature, and e the electronic charge. However, the varying concentrations of all other ions also affect the membrane potential, so that predicting $\Delta\Psi$ requires tracking the movement of the dominant counter ions, the membrane capacitance, as well as the buffering and Donnan properties of the lumenal matrix.

By their effect on the membrane potential, the proton pumping ability of the V-ATPase can be influenced by other ion pumps, such as the Na,K-ATPases as well as chloride and/or potassium channels. In addition, proton leaks and can dissipate gradients that are built up by the proton pump. Moreover, organelle shape and size are important parameters in determining membrane capacitance and, thus, acidification rates. Matters are further complicated by the osmotically driven movement of water in response to changing ion concentrations. To facilitate discussion of the various factors influencing acidification, we shall divide our discussion into three general categories: pumps, channels, and organelle shape and contents.

Ion Pumps

For our purposes, an ion pump can be characterized by its "performance surface" giving the average rate of a single pump as a function of the transmembrane ion gradient and electrical potential, denoted $J(\Delta pH, \Delta\Psi)$. To measure this surface, a comprehensive series of experiments must be performed. However, since these experiments have not yet been carried out in sufficient detail, we shall rely on models for each pump.

We constructed a mechanochemical model of the V-ATPase that predicts the proton flux as a function of environmental conditions (Grabe et al., 2000). By calibrating the model from whole vacuole patch-clamp experiments the proton pumping performance surface, $J_H(\Delta pH, \Delta\Psi)$, was computed (Fig. 2 A).

A similar mechanistic molecular model of the Na,K-ATPase does not yet exist. However, for our purposes, an accurate kinetic description will suffice. These enzymes generally localize to the

---

[1]*Abbreviations used in this paper:* MVB, multivesicular bodies; pmf, proton motive force; RRC, receptor recycling compartments.
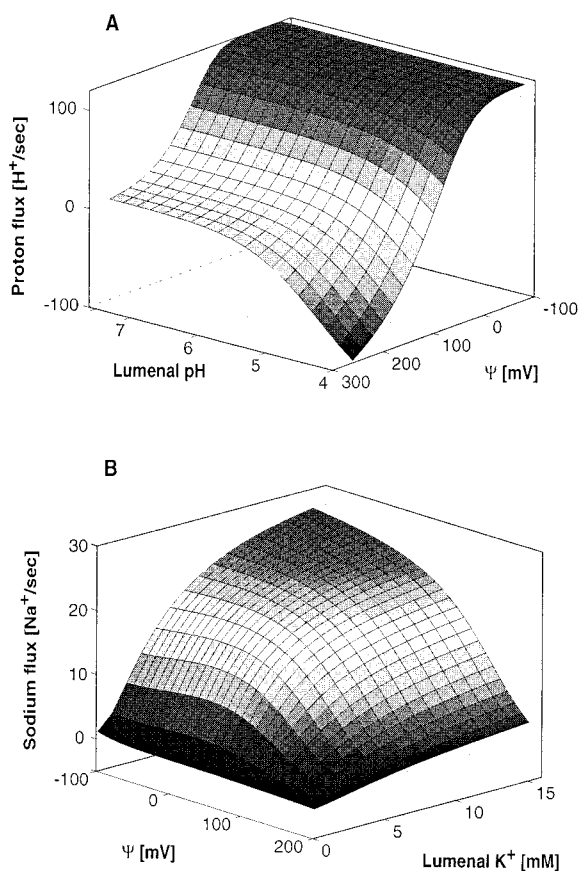
FIGURE 2. Performance surfaces. (A) The proton pumping rate [H$^+$/s] for a single V-ATPase is plotted as a function of lumenal pH and membrane potential across the bilayer. The bulk cytoplasmic pH is 7.4, but the proton concentration at the membrane is modified by a −50-mV surface potential. The free energy of ATP hydrolysis is 21 k$_B$T. In principle, the pumping surface can be measured empirically. However, in the absence of such measurements, we have computed the surface based on the mechanochemical model for the V-ATPase as described in Grabe et al. (2000). The parameters used in the computations are given in Table S1 (see *Online Supplemental Material* available at http://www.jgp.org/cgi/content/full/117/4/329/DC1). (B) The pumping rate for a single Na,K-ATPase plotted as a function of lumenal potassium concentration and membrane potential. Bulk cytoplasmic potassium and sodium concentrations are maintained constant at 140 and 20 mM, respectively. Membrane values of these concentrations are also modified by a −50-mV surface potential as in A. The free energy of ATP hydrolysis is 21 k$_B$T, and the lumenal sodium is fixed at 145 mM. The pumping profile was computed from the composite model found in *Online Supplemental Material*. See Table S2 (available at http://www.jgp.org/cgi/content/full/117/4/329/DC1) for a complete list of all parameters.

plasma membrane of cells where high turnover rates are needed to maintain low cytoplasmic sodium levels. Many kinetic models describe the pump only under this limited set of environmental conditions and generally neglect reverse reactions necessary for preserving detailed balance (Hartmann and Verkman, 1990; Sagar and Rakowski, 1994). However, the Na,K-ATPases found in organelles may not operate over a much greater set of conditions. Therefore, we shall use the more general model of Apell and Lauger, which obeys microscopic reversibility (Lauger and Apell,

1986). We have combined two extensions of this model that take into account most of the known experimental data on the potassium and sodium portions of the pump cycle (Heyse et al., 1994; Sokolov et al., 1998). From this combined model, the sodium flux (J$_{Na}$) and potassium flux (J$_K$) for an individual ATPase were determined. We have plotted the response surface for the potassium portion of the flux in Fig. 2 B. Accurate performance surfaces such as this are sufficient to predict the Na,K-ATPase's response to transmembrane ionic and potential differences. A description of both pump models along with the Matlab™ code used to compute them is given in *Online Supplemental Material*.

The performance surfaces characterize the average behavior of individual pumps. To compute acidification rates, we must know the number of active pumps. This can be estimated from electron microscopy and biochemical assays (e.g., mAb tagging). However, these estimates are difficult and often inaccurate since only the total number of pumps, not the active fraction, can be deduced from microscopy. Therefore, we shall estimate the number of active pumps in a given organelle by fitting experimental acidification curves or by matching steady-state pH values.

Before continuing, it is natural to ask how heavily our results depend upon the exact shape of the performance surfaces in Fig. 2. To address this, all simulations have been computed with simpler pump models assuming that the pump flux decreases linearly with increasing electrochemical gradient. Most of the data we fit with the nonlinear performance surface can be fit with a linear pump model. However, this necessitates significant changes in key parameters, such as the number of active pumps. Thus, for the systems examined, the exact dependence of the pumps on environmental conditions is not critical. What is important is that the pumps provide a source of ion flux, and pH regulation results from the interplay of this source with other regulatory elements to be discussed. Why then use the nonlinear pumping surfaces in Fig. 2? First, there are situations where the pump mechanism is crucial to pH regulation, such as hyperacidic organelles whose pH is below 2. Second, it is as easy to compute the regulation curves using the nonlinear pump model as with the linear model, and it does not obfuscate the role that pumps play in the overall scheme.

Channels: Chloride, Potassium, and Proton Leak

Intact bilayers are somewhat permeable to protons, but relatively impermeable to other ions. Ion-specific channels allow an organelle to equilibrate specific ions between the lumen and cytoplasm. Movement of these ions through the channel is driven by the transmembrane concentration difference and the membrane potential. The simplest model for this movement assumes that the ion and the channel do not interact during transport. In this limit, the permeability coefficient is the only relevant parameter determining the dynamics of transport. In the presence of a membrane potential, the diffusion flux of ions can be described by Eq. 2 (Hille, 1992; Weiss, 1996):

$$J_i = P_i \cdot S \cdot \frac{z_i U([C_i]_L - [C_i]_C e^{-z_i U})}{1 - e^{-z_i U}}, \qquad (2)$$

where i denotes the ionic species (Cl$^-$, K$^+$, or H$^+$), P$_i$ is the permeability of the membrane to ion i, S is the surface area of the compartment, C$_i$ is the concentration of the ion in the cytoplasm (C) or lumen (L), z$_i$ is the valance of the ion, and U is the reduced membrane potential, U = ΨF/(RT). F, R, and T have their usual meanings.

Proton movement across membranes is not well understood. Protons are permeant to intact bilayers, so it is possible that their transport is not channel mediated. It may involve a more complicated mechanism using water wires or the partitioning of weak

Parameters of Interest

Description	Units	Symbol	Value	Reference
Energy of ATP hydrolysis		ΔG_{ATP}	21 $k_B T$	Rybak et al., 1997
Cytoplasmic pH*		pH_C	7.0–7.5	Roos and Boron, 1981;Wu et al., 2000
Cytoplasmic sodium concentration	mM	Na_c^+	15	Alberts et al., 1994
Cytoplasmic potassium concentration	mM	K_c^+	140	Alberts et al., 1994
Cytoplasmic chloride concentration	mM	Cl_c^-	4	Alberts et al., 1994
Cytoplasmic ATP concentration	mM	ATP_c	5	Lauger and Apell, 1986
Cytoplasmic ADP concentration	mM	ADP_c	0.1	Lauger and Apell, 1986
Cytoplasmic phosphate concentration	mM	P_c	5	Lauger and Apell, 1986
Cytoplasmic calcium concentration	M	Ca_c^{2+}	10^{-7}	Alberts et al., 1994
Extracellular sodium concentration	mM	Na_e^+	145	Alberts et al., 1994; Rybak et al., 1997
Extracellular potassium concentration	mM	Ke^+	5	Alberts et al., 1994
Extracellular chloride concentration	mM	Cl_e^-	110	Alberts et al., 1994
Extracellular calcium concentration	mM	Ca_e^{2+}	2.5-5	Alberts et al., 1994
Extracellular phosphate concentration	mM	P_e	1	Vander et al., 1985
Bilayer capacitance	$\mu F/cm^2$	C_0	1	Israelachvili, 1992
Golgi complex buffering capacity	mM/pH	β_G	10, 40	Farinas and Verkman, 1999; Wu et al., 2000
ER buffering capacity	mM/pH	ER	6	Wu et al., 2000
Endosome buffering capacity	mM/pH	EN	50	Rybak et al., 1997
Chloride permeability	cm/s	P_{Cl}	1.2×10^{-5}	Hartmann and Verkman, 1990
Proton permeability	cm/s	P_p	$4.8–0.67 \times 10^{-3}$	Van Dyke and Belcher, 1994
Golgi complex volume	cm^3	V_G	6×10^{-12}	Ladinsky et al., 1999
Endosome volumes	cm^3	V_{EN}	$88–0.7 \times 10^{-15}$	Van Dyke and Belcher, 1994
Golgi complex surface area	cm^2	S_G	8×10^{-6}	Ladinsky et al., 1999
Endosome surface area	cm^2	S_{EN}	$1–0.06 \times 10^{-8}$	Van Dyke and Belcher, 1994

Names and values of relevant physiological parameters.

*We occasionally refer to $pH_C = 7.4$ as a typical cytoplasmic pH. This value may appear high in relation to older literature (Roos and Boron, 1981), but it is in line with many of the most recent fluorescence experiments (Wu et al., 2000).

acids into the bilayer (Paula et al., 1996; Hill et al., 1999). Additionally, voltage-gated proton channels exist in the plasma membrane of certain cell lines, where they are responsible for extruding acid from the cytoplasm (DeCoursey and Cherny, 2000). Whether such channels are functional in organelles is not known. If transport is mediated by voltage-gated channels, the mathematical description above may be inappropriate for the proton flux. Lacking a concrete description of the passive proton flux, we continue with the simple treatment of Eq. 2. As we shall see, this model fits experimental data quite well.

Net proton movement across the membrane is a competition between V-ATPase pumping and channel-mediated leaking. In general, high physiological concentrations of counter ions lead to counter ion movement that is much faster than either of these two processes. This follows from Eq. 2 since the flux is proportional to the difference in ionic concentrations. Thus, no new time scale is introduced into the problem by incorporating channels; the dynamics of acidification will primarily be determined by the proton movement.

We deduce proton permeabilities from data associated with each of the experiments examined. The permeability value for chloride, listed in Table I, is taken from measurements on non-voltage-activated channels residing in the plasma membrane. We shall assume that the permeabilities of the other counter ions have this same value. The rate of acidification is unaffected by variations in the permeabilities as long as the permeability does not become so small as to place counter ion movement on the same time scale with proton movement.

Organelle Properties: Buffering Capacity, Donnan Potential, Osmotic Effects, and Shape

The lumenal matrix of an organelle is composed of a polymeric network of proteins. These proteins tend to be negatively charged, and can buffer changes in pH. The negative charge of the matrix is balanced by mobile counter ions which generate a Donnan potential. The volume and surface area of the organelle also play an important role in determining concentrations, membrane potential, and membrane fluxes. These parameters are among the most difficult to quantify primarily because of the large variations in organelle size and shape. Electron micrographs show that even vesicles from purified populations exhibit a broad distribution of volumes and surface areas (Belcher et al., 1987). For the organelles studied here, we have tried to find the most current measurements of these two parameters; a list is given in Table I. When values were uncertain, these parameters were varied to determine the best fit to experimental data.

The buffering capacity, β (units: mol/pH), is the degree with which the lumenal matrix is able to bind protons from solution. Since the matrix composition is quite complex, the buffering capacity can only be determined experimentally by biochemical analysis. At a particular lumenal pH, this analysis determines the constant of proportionality between the change in proton concentration of the lumen and the change in pH, $\Delta[H^+] = \beta \cdot \Delta pH$. In general, this relation is not linear since β depends on the lumenal pH. For pH values near 7, the buffering capacities for the ER and Golgi complex are found to be approximately constant, varying between 6–40 mM/pH unit. Similar experiments

have been performed on endosomes and lysosomes in which the buffering capacity did not appear to be constant (see Figure S5; Van Dyke, 1993; Van Dyke and Belcher, 1994). For each simulation, the buffering capacity was determined from experimentally measured values. This is discussed in more detail in *Online Supplemental Material* and the review by Roos and Boron (1981).

The membrane potential affects the flow of ions across lipid membranes and biases the distributions of those ions at steady state. Electroneutrality requires that no net charge exists in any small volume; the membrane potential arises from the microscopic deviation from electroneutrality at a lipid boundary. Physiological models generally exploit the concept of electroneutrality to solve for the membrane potential without detailed information about the electrical makeup of the cell. This requires that the ionic currents crossing the membrane sum to zero at all times. This constraint results in a single algebraic equation whose root gives the membrane potential. Additionally, Hodgkin-Huxley type models relate the electrical activity of the cell to the movement of ions across the membrane by a differential equation for the time dependence of the potential (Hodgkin and Huxley, 1952). Both of these approaches ignore two important features that strongly influence the membrane potential: (1) fixed lumenal charges, and (2) charged lipid headgroups in the bilayer. To include these elements, a physical model of the membrane potential in terms of ionic charge distributions is required.

Poisson-Boltzmann models (more specifically, Gouy-Chapman methods) provide one approach for determining the electrical profile and ion concentrations near the lipid bilayer. To accurately determine these profiles all charged solutes must be included in the calculation (McLaughlin et al., 1981). This is beyond the scope of the present model, since we track only the dominant counter ion concentrations. Motivated by Rybak et al. (1997), we give an explicit form for the membrane potential across the bilayer in terms of the excess charge inside the organelle. We assume that the net charge localizes to the lumenal leaflet, so that we can treat the membrane as a parallel plate capacitor. This is valid since the radius of curvature of organelle surfaces is quite small compared with their thickness. The potential drop across the bilayer is written as Eq. 3:

$$\Delta \Psi = \frac{F}{C_0} \cdot \frac{V}{A} \cdot \left(\underbrace{\frac{\sum_i v_i \cdot [\text{cations}]_i - \sum_i v_i \cdot [\text{anions}]_i}{1}}_{} \right.$$
$$\left. + \underbrace{\frac{\beta \cdot (pH_C - pH_L)}{2}}_{} - \underbrace{\frac{B}{3}}_{} \right),$$
(3)

where A is the surface area of the membrane, C_0 is the capacitance per unit area of the membrane ($C_0 \cdot A$ is the total capacitance of the membrane), V is the volume of the organelle, F is Faraday's constant, and the numbered terms giving the concentrations of charged particles are as follows. (1) Sum of ions (chloride, potassium, sodium, and calcium) weighted by their stoichiometric coefficient n (e.g., n = 1 for monovalent and 2 for divalent ions). (2) Total amount of buffered and free protons in the lumen. β is the buffering capacity. We assume that protons do not contribute to the membrane potential when the lumenal pH is equal to the cytoplasmic pH. When the buffering capacity is not constant, this term must be integrated to give the total number of lumenal protons contributing to the membrane potential. (3) Molar concentration of all impermeant charges. This term primarily represents fixed negative protein charges trapped in the lumen; however, fixed cations (such as calcium), which keep the lumenal matrix condensed, may reduce the magnitude of this term (Verdugo, 1991). Experimental estimates of these con-

centrations vary by >100 mM from organelle to organelle. Some of these values are listed in Table I. In each simulation, this parameter is estimated from resting pH values in the absence of proton pumping or from best fits as a variable parameter.

Changes in the membrane potential, according to Eq. 3, come about as a direct consequence of changes in the lumenal concentrations of those ions being tracked. The constant charge density term (B) sets the zero point of the membrane potential and biases the lumenal proton concentration as well as the ionic concentrations in term 1. Large values of B have been implicated in the acidic pH that lysosomes maintain in the absence of proton pumps (Moriyama et al., 1992). A recent study using a similar model for the membrane potential has shown good agreement with experimentally predicted membrane potentials (Endresen et al., 2000).

To account for the effects of surface charge, we include a phenomenological potential difference between the bulk cytoplasm and the organelle's outer leaflet, $\Delta \Psi_{C,0}$, and the bulk lumen and the inner leaflet, $\Delta \Psi_{L,0}$ (Hille, 1992). These potentials modify all ionic concentrations at these surfaces by a Boltzmann factor:

$$[C_i]_{L,0} = [C_i]_L \cdot \exp\left(\frac{-z_i F \Delta \Psi_{L,0}}{RT}\right)$$
$$[C_i]_{C,0} = [C_i]_C \cdot \exp\left(\frac{-z_i F \Delta \Psi_{C,0}}{RT}\right),$$
(4)

where the surface concentrations are denoted by a zero subscript. Given the typical surface potentials measured for negative phospholipid bilayers bathed in frog Ringer's solution, this theory predicts Ca^{2+} surface concentrations to be 20–10^4 times higher than bulk values (Hille, 1992). These modified concentrations are the values that must be used for computing current flow through membrane channels and pumps. For example, surface concentrations must replace the bulk values in Eq. 2 to solve for the instantaneous flow of ions across the membrane. In general, as the lumen is acidified and ionic concentrations change, $\Delta \Psi_{L,0}$ will also change. We assume that the change in net ionic concentrations is small enough to ignore this effect.

The lipid compositions of cellular membranes are inherently asymmetric, with the cytoplasmic leaflet tending to be more negatively charged due to the preponderance of acidic lipids (Rothman and Lenard, 1977). The surface potential depends strongly on this composition. Vesicles containing 33% acidic lipid in 100 mM monovalent salt concentrations have surface potentials about −50 mV (McLaughlin, 1989). The most relevant physiological measurements of surface potentials have been performed on the plasma membrane. Cahalan and Hall (1982) observed a cytoplasmic surface potential of −30 mV in frog nerve cells. Lacking specific information about the lipid composition of the organelles studied, we assign reasonable, yet arbitrary, values of $\Delta \Psi_{C,0}$ = −50 mV and $\Delta \Psi_{L,0}$ = 0 mV. We retain these values throughout our study and examine the sensitivity of our model to these parameters in Table V. For cytoplasmic surface potentials in the range of −30 to −50 mV, we expect surface concentrations of divalent and monovalent cations to be ~5–50 times higher than bulk concentrations.

Although it is generally accepted that surface charges influence ion concentrations near the membrane, this effect on the operation of pumps and channels is not well characterized. The charges on the transporter itself could affect the local ion concentration much more than the nearby lipids. Additionally, the V-ATPase, like many transporters, is quite large, and the ion binding sites may be more than a Debye length away from the closest membrane lipids. Thus, electric fields generated at the membrane will be screened at the transporter, and ionic concentrations may not be very different from the bulk solution. These issues can be answered only by experiments. For the model trans-

porters used here, we discuss how changes in surface potential affect flux rates in the *Online Supplemental Material*. There, we show that when the surface potential is zero, predicted permeability coefficients increase by a factor of 2–3, and proton pumping rates decrease by less than a factor of 2. Nevertheless, the overall theme of our discussion remains unchanged.

Experimental measurements of the membrane potential are between the bulk cytoplasm and the bulk lumen. Using the model just outlined, this total potential difference is given by Eq. 5:

$$\Delta\Psi_{Total} = \Delta\Psi + (\Delta\Psi_{C,0} - \Delta\Psi_{L,0}) \tag{5}$$

All reported membrane potentials refer to the total membrane potential. Using the definitions in Eq. 5, $\Delta\Psi_{Total} > 0$ will drive anions into the lumen and cations out.

Differences in ion concentrations across the membrane give rise to an osmotic pressure that drives water across the membrane. This effect will change the total volume of the organelle and may influence the lumenal pH. The flux of water into the lumen can be written as Eq. 6:

$$J_W = P_W \cdot S \cdot \left(\sum_i \frac{\phi_i}{a_i} \cdot [C_i]_L - \Phi_C \right), \tag{6}$$

where Φ_C is the osmolarity of the cytoplasm or external solution and P_W is the permeability. The water permeability of endosomes isolated from rat kidney is $P_W \approx 0.052$ cm/s (Lencer et al., 1990). For ionic species i, ϕ_i is the osmotic coefficient, a_i is the solute activity, and $[C_i]_L$ is the lumenal concentration. The osmolarity of the cytoplasm is constant with a typical value of $\Phi_C \approx 291$ mM. We assume that vesicles are initially in osmotic equilibrium. This allows us to assign an osmolarity for those lumenal solutes that are impermeable to the membrane. The osmotic coefficient of the charged solutes is taken as 0.73.

Numerical Solutions

With Eqs. 1–6 we can construct a model organelle and write a set of balanced equations that keep track of the movement of ions across its membrane. A typical set of equations are as follows:

$$(a) \quad \frac{dH^+}{dt} = N_{H^+} \cdot J_{H^+}(pH_L, \Psi) - P_{H^+} \cdot S \cdot \frac{U([H^+]_L - [H^+]_C \cdot e^{-U})}{1 - e^{-U}}$$

$$(b) \quad \frac{dK^+}{dt} = -2 \cdot N_{Na,K} \cdot J_{Na,K}(Na_L, K_L, \Psi) -$$

$$P_{K^+} \cdot S \cdot \frac{U([K^+]_L - [K^+]_C \cdot e^{-U})}{1 - e^{-U}}$$

$$(c) \quad \frac{dNa^+}{dt} = +3 \cdot N_{Na,K} \cdot J_{Na,K}(Na_L, K_L, \Psi) \tag{7}$$

$$(d) \quad \frac{dCl^-}{dt} = P_{Cl^-} \cdot S \cdot \frac{U([Cl^-]_L - [Cl^-]_C \cdot e^{-U})}{1 - e^{-U}}$$

$$(e) \quad \Psi = \frac{F}{C_0} \cdot \frac{V}{S}$$

$$\{[Na^+]_L + [K^+]_L(-[Cl^-]_L + \beta(pH_L) \cdot (pH_C - pH_L) - B)\}$$

$$(f) \quad \frac{dpH}{dt} = -\frac{1}{\beta(pH_L)} \cdot \frac{d[H^+]}{dt}$$

The fluxes, J_{H^+}, J_{Na^+}, and J_{K^+}, and the buffer curve, β, are imported numerical functions from the pump performance surfaces and the titration data, respectively. As always, brackets denote molar quantities, whereas stand alone symbols represent number of ions. Time varying variables refer to lumenal quantities, all of

which are coupled by the membrane potential. The equations were solved using Berkeley Madonna™ with the Rosenbrock algorithm for stiff differential equations (Press, 1997). All simulations start with an initial membrane potential of zero, and negative Donnan particles are masked by an equal concentration of lumenal cations. Initial lumenal concentrations of counter ions do not affect steady-state values since they are allowed to diffuse until their Nernst potential is zero. In the next section we solve these equations for various experimental configurations.

Online Supplemental Materials

Detailed calculations and further discussion of specific topics are available online at http://www.jgp.org/cgi/content/full/117/4/329/DC1. These include all of the following: V-ATPase and Na,K-ATPase pumping profiles, buffering capacity, and surface potentials. This site also contains the computer program used to compute organelle acidification rates. It is easy to use, and can be tailored by the user for particular experimental situations; it requires the commercial software Berkeley Madonna™. The Matlab™ code used to compute the pumping profiles in Fig. 2 can be downloaded.

R E S U L T S

Using the model outlined above, we examined experiments performed on reconstituted organelles and on intact cells. Reconstitution experiments make it possible to measure ATP-dependent acidification of organelles that have been incubated in solutions lacking ATP. These experiments give important information on the kinetics of acidification. However, it is not clear that the process of reconstitution does not drastically alter the biochemical makeup of the organelle. Experiments performed on intact cells can also provide kinetic information, and they are much less invasive than reconstitution experiments. In this section we show that our model is in quantitative agreement with reconstitution experiments, and highlight areas of pH regulation that our model can help elucidate. We also examine data recorded from intact cells to address several outstanding questions in pH regulation.

Calibration: The Model Accurately Describes
the Acidification of Organelles

It is necessary to confirm the ability of our model to describe acidification before attempting to draw general conclusions from ambiguous data. We begin by analyzing the ATP-dependent acidification of rat kidney endosomes recorded by Shi et al. (1991). Endosomes were reconstituted in a solution devoid of ATP, effectively turning off the V-ATPase. Next, ATP was reintroduced into the external solution and the subsequent acidification of single endosomes was measured. These experiments form a particularly good benchmark because external variables were tightly controlled in the reconstituted medium and the acidification measurements were performed on single endosomes rather than a population. When modeling a single organelle, model parameters
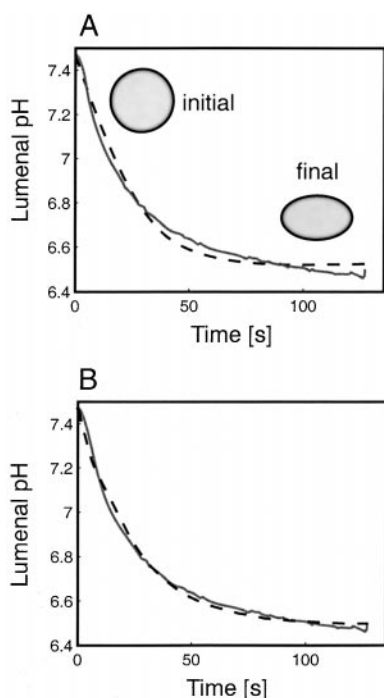
Figure 3. (Top) Modeling the ATP-dependent acidification of a single endocytic vesicle from rat kidney. The model (dashed) is compared against the experiments (solid) of Shi et al. (1991). Simulations include the effects of V-ATPases, proton leaks, passive potassium channels, Donnan equilibrium, and buffering capacity. Table II lists all parameters. (A) Acidification with a constant buffering capacity of 40 mM/pH, as reported by Shi et al. (1991). The vesicle is initially in osmotic equilibrium with an external solution having an osmolarity of 291 mM. The efflux of potassium upon acidification results in a decrease of osmotically active particles; thus, shrinking occurs. Cross-sectional areas of the initial spherical vesicle and an ellipsoid corresponding to the final volume of the vesicle are drawn to scale. The osmotic activity of the protons and the potassium ions is given in Table I. The shapes of the acidification curves with and without water flow are indistinguishable at this scale.(B) An approximation to the buffering data reported by Van Dyke and Belcher for MVB endosomes was used to model the acidification curve in A. This buffering curve can be seen in Figure S5 (available at http://www.jgp.org/cgi/content/full/117/4/329/DC1). The lumenal buffering capacity has a noticeable influence on the models ability to fit the data.

such as buffering capacity and pump numbers can be interpreted as literal properties of the organelle rather than average properties of a population of organelles.

In Fig. 3 (A and B), we modeled the acidification of an endosome using a constant (Fig. 3 A) and a variable (Fig. 3 B) buffering capacity. The simulation is of a spherical vesicle 163 nm in diameter containing proton pumps and leaks, potassium channels, and trapped negative charges. The experiment (solid line) was performed in a solution of 100 mM potassium, and we assume that potassium is permeant to the membrane. The diameter, number of proton pumps, and proton permeability were varied to give the best fit to the data. At time zero, the lumen was acidified from its initial pH

of ~7.4 by turning on the ATP-dependent V-ATPase. In both simulations, the final membrane potentials were ~15 mV, the energetic equivalent of ΔpH ≈ 0.3. This justifies the authors' assertion that the membrane potential is not appreciable when potassium is free to diffuse across the bilayer.

We investigated two parameters that affect the shape of the acidification curves: buffering capacity and osmotic fluid flow. In Fig. 3 A, we used a constant lumenal buffering capacity of 40 mM/pH unit, as reported by Shi et al. (1991). The buffering curve used in Fig. 3 B was adapted from endosomal data recorded by Van Dyke and Belcher (1994; see Figure S5 available at http://www.jgp.org/cgi/content/full/117/4/329/DC1). At the same volume, the variable buffering capacity gives a noticeably better fit to the data, indicating the importance of buffering in describing pH dynamics. Water channels were also included in the simulation to allow volume change while the surface area remained constant. We assumed that the spherical vesicle was initially in osmotic equilibrium and that the osmolarity of the external medium was 291 mM, a typical cytoplasmic value. From the shapes in Fig. 3 A, we see that endosomal shrinking occurs as buffered protons expel osmotically active potassium ions. The model predicts an 11% decrease in volume, which is in agreement with the authors' estimate of a decrease of less than 15%. Interestingly, the change in volume during acidification has no effect on the shape of the curve in Fig. 3 A: the curves with and without water exchange are virtually indistinguishable.

The goodness of the fits, coupled with the constraints imposed by the experiments, indicate that the model can accurately represent the physical situation. The buffering capacity plays a dominant role in the dynamics of acidification, and our ability to extract reliable numbers from fits depends upon the fidelity with which the buffering curves are known. We predict shape changes due to osmotic shrinking, but this effect has little influence over the shape of the endosomal acidification curves. Finally, the predicted steady-state pmf's are relatively small, indicating that the V-ATPase proton
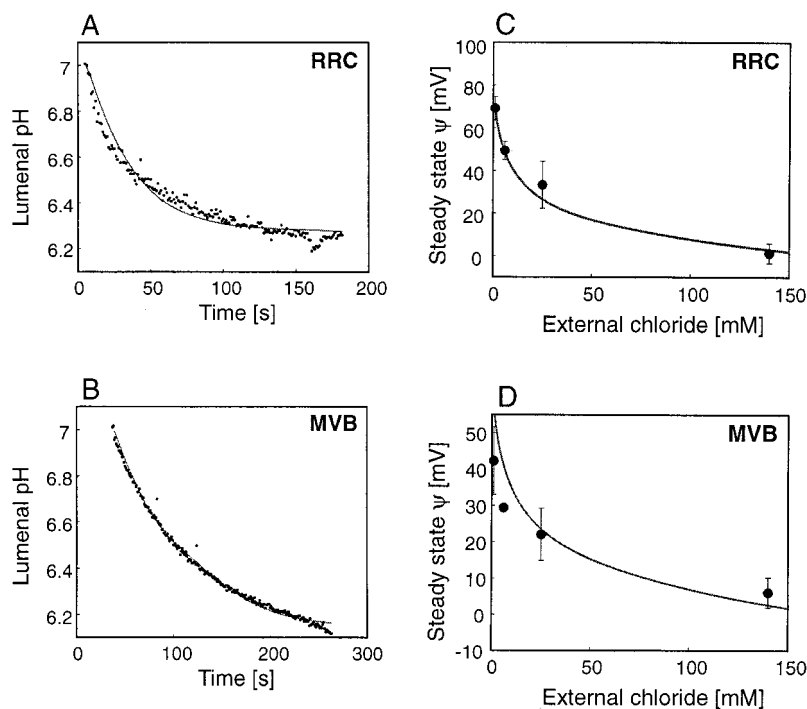
FIGURE 4. (Top) Modeling the ATP-dependent acidification of vesicles in rat liver from two different stages of endocytosis. Model predictions are shown in solid lines and the experimental data points were provided by Van Dyke and Belcher (1994). Controls include the following: V-ATP-ases, proton leaks, passive chloride channels, passive potassium channels, Donnan equilibrium, and buffering capacity. See Table III for all parameters. (A) The acidification of the receptor recycling compartment (RRC). The buffering capacity is extrapolated from experimental values determined by Van Dyke and Belcher. (B) Acidification of the much larger multivesicular bodies (MVB). Fitting the data required a pump density on the MVB vesicles approximately eight times greater than the RRC vesicles. (Bottom) Steady-state membrane potential as a function of external chloride concentration. The presence of chloride enhances acidification by allowing chloride to enter the vesicle to reduce the membrane potential against which the pump must operate. Both C and D show that increasing the external chloride concentration is an effective way to reduce the resting membrane potential. (C) For the RRC population, the dependence of the membrane potential on the external chloride concentration matches experimental observations with the same parameters for the simulations in A. (D) A fivefold decrease in the number of proton pumps relative to B is required to describe the MVB population's dependence on the external chloride concentration.

pump is not working close to thermodynamic equilibrium, which corresponds to Δpmf $\approx$ 4.5 pH units (Grabe et al., 2000). This suggests that the steady-state pH in endosomes, lacking Na,K-ATPases, is the result of a balance between proton pumping and leaking.

The Model Provides a Consistent Theory of pH Gradient and Membrane Potential

A satisfactory theory of pH regulation requires an understanding of both the electrical- and concentration-dependent portions of the pmf across the organelle bilayer. Here, we model experiments that monitor membrane potential in addition to acidification. A similar class of experiments to those of Shi et al. (1991) involves measuring the fluorescence from whole populations of a specific organelle. One acidification curve is measured for the entire population, and it is assumed that this curve represents the dynamics of an average vesicle in that population. Van Dyke and Belcher (1994) have performed a number of experiments on three distinct endosomal populations extracted from normal rat kidney cells. We modeled their acidification data from the receptor recycling compartments (RRC) and multivesicular bodies (MVB) where they report average values for the surface area, volume, and pump leak rate for each of these populations. In addition, they show that the buffering power of the lumenal matrix depends strongly upon the value of the internal pH

(see *Online Supplemental Material* available at http://www.jgp.org/cgi/content/full/117/4/329/DC1).

Fig. 4 (A and B) shows the acidification of vesicles in the presence of chloride and potassium channels, fixed negative lumenal proteins, and proton pumps and leaks. For this calculation, we used the buffering curves from Figure S5 (available at http://www.jgp.org/cgi/content/full/117/4/329/DC1); other parameters for these simulations and the percent deviation from measured values are given in Table III. As in the Verkman experiments, large proton permeabilities, on the order of 10^{-3} cm/s, suggest that the ratio of the leak rate to the pump rate is the major determinant of steady-state pH. Table III shows that the model parameters are comparable to the average experimental values. The RRC parameters are consistently closer than the MVB parameters to the measured values. However, the most inaccurate MVB parameter (volume) is only a factor of 1.7 larger than the reported value.

To investigate the role of counter ions, Van Dyke and Belcher (1994) varied the external chloride concentration and measured the resulting steady-state membrane potential. When the membrane is permeable to chloride, Eq. 2 predicts that changes in the external chloride concentration will affect the steady-state distribution of the ion across the membrane. Subsequently, the membrane potential will change according to Eq. 3. Fig. 4 (C and D) shows that the model describes the membrane potential's dependence on the external

Parameter	Units	Panels A and C	RRC	Panels B and D	MVB
H$^+$ permeability	cm/s	0.60×10^{-3}	-10	2.0×10^{-3}	-58
Surface	cm^2	0.45×10^{-9}	-24	13.6×10^{-9}	32
Volume	cm^3	0.07×10^{-14}	0	15×10^{-14}	70
Donnan particles	mM	7	–	9	–
Buffering capacity	mM/pH			see Figure S5	

List of parameters used in the simulations in Fig. 4. Simulations in panels A and B were performed with 10 mM bulk chloride and potassium, whereas the potassium was 140 mM in panels C and D. The number of V-ATPase proton pumps in panels A and C was 2, whereas in panels B and D had 354 and 70 pumps, respectively. The columns RRC and MVB are the percent differences between model parameters and the average values recorded by Van Dyke and Belcher (1994). The external pH was held fixed at 7.0 for all simulations.
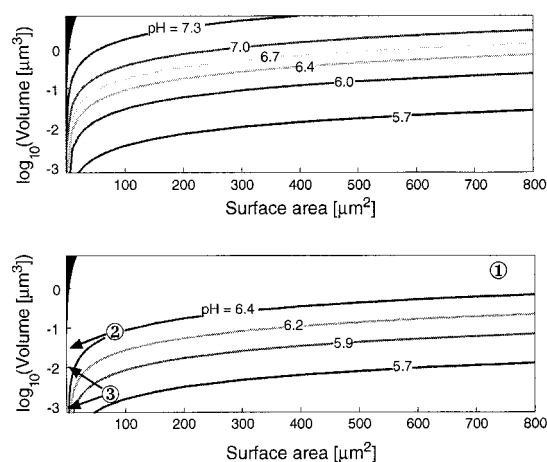

FIGURE 5. The effect of surface area and volume on steady-state pH. Simulations include V-ATPases, proton leaks, chloride channels, Donnan equilibrium (120 mM), and buffering capacity (10 mM/pH unit). The density of proton pumps and the proton permeability were held constant at 10^9 pumps/cm^2 and 10^{-4} cm/s, respectively. Constant steady-state pH is plotted as a function of the surface area and volume in the absence (top) or presence (bottom) of 5 mM chloride (140 mM of impermeant potassium is assumed to be present internally). The bulk cytoplasmic pH is 7.4. Even at low counter ion concentrations, the effect of changes in the vesicle shape on the steady-state pH is small. The bottom panel shows highlighted regions corresponding to reported surface areas and volumes for specific organelles: (1) normal rat kidney Golgi complex (Ladinsky et al., 1999); (2) rat kidney endosomes (Shi et al., 1991); and (3) rat liver endosomes (Van Dyke and Belcher, 1994).

chloride concentration quite well. As the chloride concentration is increased, a greater lumenal concentration of chloride counter balances the presence of protons, thus reducing the membrane potential.

One set of parameters described both sets of RRC data, yet the MVB data required an eightfold decrease in the number of proton pumps to describe the dependence of membrane potential on external chloride concentration. Whether such variations are to be expected from trial to trial is not clear. Interestingly, panels A, C, and D of Fig. 4 have very similar pump densities ($\sim$50 pumps/μm^2) indicating that no active sorting of the proton pump occurs between these populations. However, the MVB simulation in Fig. 4 B required a pump density of 270 pumps/μm^2. More consistent fits that agree over more data sets are required before we can make any claim about sorting events. Fig. 4 (C and D) shows that our model quantitatively describes the dependence of the membrane potential on external ion concentrations. The ability to fit both the membrane potential and acidification data with the same set of parameters in Fig. 4 (A and C) suggests that the model provides a consistent theory of both components of the pmf.

Morphological Changes Alone Cannot Account for the Decrease in pH along the Secretory Pathway

In the absence of proton leaks, the steady-state pH of a model vesicle depends strongly on its shape and size (Rybak et al., 1997). This dependence can be seen from Eq. 3 in which the membrane potential is proportional to the ratio of the volume to the surface area. When this ratio is small, we expect to see a reduction in membrane potential and lower steady-state pH values. Can this effect alone explain the decrease in pH along the secretory pathway?

We have not been able to find data to directly model this question. However, we note that many experiments performed on intact cells have shown that significant

proton leakage occurs in many major organelles (Farinas and Verkman, 1999; Schapiro and Grinstein, 2000; Wu et al., 2000). Therefore, when revisiting the analyses of Rybak et al. (1997) we included a proton leak when exploring the effects of vesicle shape and size.

In Fig. 5, we plotted the steady-state pH of a nonequilibrium system containing a constant density of proton leaks and proton pumps. The final pH is plotted as a function of surface area and the logarithm of volume. In the bottom panel of Fig. 5, numbers indicate experimentally measured surface areas and volumes of several different types of organelles. In the absence (Fig. 5, top) and presence (Fig. 5, bottom panel) of chloride channels, there is very little change in the final pH as the shape changes from small spherical endosomes and secretory granules (near population 1) to large floppy Golgi complex (population 3). Both panels exhibit pH changes of one unit over the range of physiological shapes, as also reported by Rybak et al. (1997). However, this effect would only explain pH variations in the cell if small vesicles and endosomes had much more surface area than is seen in electron micrographs.

The model predicts when proton leaks are present, changes in volume and surface area alone cannot account for the wide range of pHs seen in cellular organelles. This suggests that some other mechanism,

such as the sorting of proton pumps or proton leaks, is the dominant factor in regulating lumenal pH.

Permeability to Multiple Counter Ions Decreases Changes in Golgi Complex pH

Our goal was to apply the model to the data recorded from intact cells to predict Golgi complex proton permeability values and explore the role of counter ions in regulating Golgi complex pH. Through the biochemical manipulation of intact and membrane permeabilized cells, Wu et al. (2000) were able to affect intracellular conditions and record subsequent changes in organelle pHs. Thus, they are able to carry out experiments similar to the reconstitution studies discussed above. We modeled two different experiments aimed at understanding proton leak and counter ion regulation. First, in the presence of bafilomycin, a potent inhibitor of V-ATPase, the cytoplasm was acid loaded by externally pulsing membrane permeable NH_4 under sodium-free conditions. The absence of sodium inhibits Na^+/H^+ exchange across the plasma membrane thereby keeping the cytoplasm acidic. After NH_4 washout, sodium was reintroduced, and the alkalinization of the cytoplasm and Golgi complex was measured over time. Since these experiments lack functional proton pumps, the proton permeability can be determined from the rate of alkalinization. Second, the role of counter ions was investigated in membrane permeabilized cells in Ringer's solution. The pH of the Golgi complex was recorded as the external solution was replaced with a chloride-free Ringer's solution.

The experimental information available is too sparse to let us address the dynamic nature of most organelles. Therefore, in the following analysis, we ignore the dynamic nature of the endomembranes. For example, we assume constant volumes, surface areas, and numbers of active pumps. We also ignore the biochemical differences between the trans, medial, and cis portions of the Golgi complex. This simplification is dictated by the fact that pH-sensitive dyes localized to the Golgi complex are spread throughout the entire network, so that the experimental recordings that we model are already averaged over the entire compartment.

In Fig. 6, we examined both the counter ion regulation (main graph) and proton leak (inset) experiments. The determination of the Golgi complex proton permeability came from the experiment in the inset. Since proton pumping was experimentally inhibited, the simulation lacks V-ATPases. At time zero, the cytoplasmic pH begins to alkalinize from the reintroduction of sodium to the external solution (Fig. 6, black circles). The Golgi complex pH rises in response to the change in proton gradient across the Golgi complex membrane (Fig. 6, open squares). Modeling the Golgi complex pH, we are able to predict the rate of alkalization of the Golgi com-
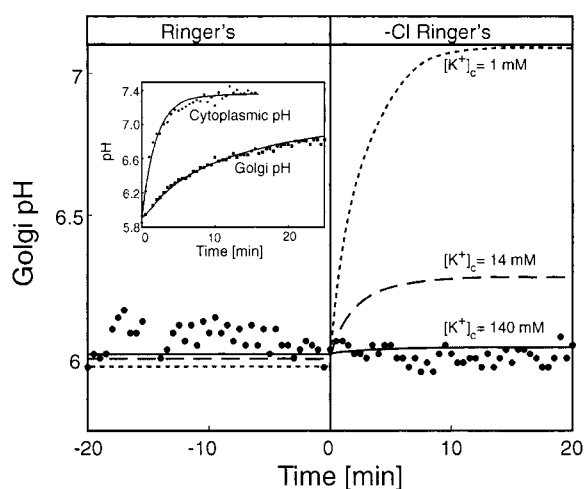

FIGURE 6. Counter ion regulation of Golgi complex pH in living HeLa cells. Wu et al. (2000) have shown that the steady-state pH of the Golgi complex is not affected by removal of chloride from the cytoplasmic solution (solid circles). These simulations include V-ATPases, proton leaks, passive chloride channels, passive potassium channels, Donnan equilibrium, and buffering (see Table IV for parameter values). At time zero, the external chloride is removed. Three theoretical curves are shown with increasing counter ion concentration. When the bulk potassium concentration is 1 mM (dotted line), the lumenal pH rises half a pH unit in response to the removal of chloride. The presence of as little as 14 mM counter ion concentration (dashed line) significantly suppresses pH changes because of chloride removal, whereas the pH change in the presence of 140 mM counter ion concentration (solid line) is imperceptible. This last case is most likely if the membrane is permeable to potassium as well as chloride. (Inset) Determination of the passive leak of protons out of bafilomycin-inhibited Golgi complex. The cytoplasm has been preacidified in sodium-free conditions that inhibit plasma membrane Na^+/H^+ exchangers. At time zero, sodium is reintroduced, and the cytoplasmic pH quickly rises due to the exchangers. This experimental curve (circles) is described by a single exponential (solid line). The Golgi complex response to the rise in cytoplasmic pH (solid line) is then fit, using the model, to the experimentally measured data (solid circles). We estimate the permeability constant of the Golgi complex to be P = 8.1×10^{-6} cm/s. The Golgi complex volume and surface area are estimated from the detailed EM tomography experiments performed by Ladinsky et al. (1999). These measurements were performed on a different cell type, and they may not be representative of the Golgi complex from HeLa cells. Since the characteristic time scale for a passive channel is given by the quantity P×(surface area), errors in the estimate of the surface area lead to uncertainties in our prediction of the permeability constant.

plex in response to the increase in cytoplasmic pH (Fig. 6, solid line). The Golgi complex leak is modeled well by a simple passive channel. Using the volume and surface area measured by Ladinsky et al. (1999), we predict a proton permeability of 8.1×10^{-6} cm/s. This value for the proton permeability is used in the main figure to examine chloride counter ion effects.

The external chloride analysis discussed above demonstrated that cytoplasmic counter ion concentrations can have dramatic effects on the membrane potential

and, consequently, on the lumenal pH. The main graph of Fig. 6 shows the resting pH of a Golgi complex in a plasma membrane compromised cell. At time zero, the external solution is replaced by a chloride-free Ringer's solution, effectively decreasing the cytoplasmic chloride from 20 to 0 mM. From our analysis in Fig. 4 (C and D), we expect the Golgi complex membrane potential to increase. After this increase in pmf, the V-ATPase pumping rate should slow, causing the lumen to alkalinize, yet experimentally the pH remains unchanged (Fig. 6, black circles). This can be explained two ways. The Golgi complex is either impermeable to chloride or permeable to chloride and at least one other dominant counter ion. Using the model, we explored the latter possibility. Three separate simulations with differing levels of cytoplasmic counter ion concentration were fit to the data. In the presence of only 1 mM additional counter ion, we predict a noticeable alkalization of the Golgi complex, ΔpH > 0.5 (Fig. 6, dotted line). The presence of a 14-mM cytoplasmic concentration counter ion (Fig. 6, dashed line) strongly suppresses changes in the lumenal pH upon removal of chloride. However, a counter ion concentration of at least 140 mM (Fig. 6, solid line) is required to eliminate any noticeable change in the Golgi complex pH.

Our analysis suggests that if the Golgi complex membrane is permeable to chloride ions, then it is also permeable to potassium. This conclusion is consistent with recent Golgi complex experiments (Schapiro and Grinstein, 2000). The fidelity with which the model reproduces the experimental data suggests that our treatment of the regulatory elements present in the Golgi complex is accurate. We predict the proton permeability of the Golgi complex to be 8.1×10^{-6} cm/s. However, this value depends upon many organelle characteristics that are difficult to quantify, such as volume, surface area, and bilayer surface potential.

Can the Na,K-ATPase Limit Acidification in the Early Endosome through Increasing the Membrane Potential?

Endosomes maintain acidic internal pHs to ensure proper sorting of receptors and ligands during endocytosis. Two subpopulations of endosomes can be identified based on their function and capacity for acidification. Early endosomes are responsible for the rapid recycling of receptors, whereas late endosomes are required for transporting cargo on to lysosomes. Late endosomes maintain more acidic lumen than early endosomes. The use of ouabain, an inhibitor of Na,K-ATPase, enhances the acidification of early endosomes both in vivo and in vitro (Cain et al., 1989; Fuchs et al., 1989). The electrogenic Na,K-ATPase is thought to inhibit acidification by increasing the membrane potential across the bilayer. A greater membrane potential, and hence greater pmf, decreases the proton pumping

rate of the V-ATPase, which results in a more alkaline lumen. Rybak et al. (1997) have attempted to quantify this hypothesis by computing equilibrium solutions of vesicles containing V-ATPases, Na,K-ATPases, and many of the regulatory elements considered here. We take this analysis one step further and use our kinetic model to simulate the dynamics of acidification in an attempt to shed more light on the feasibility of this proposed mechanism. It should be noted that some endosomes appear to be insensitive to ouabain (Teter et al., 1998). Thus, the mechanism we now examine may not be a universal property of all cell lines.

Cain et al. (1989) have measured the acidification of endosomes in single intact cells both in the presence and absence of ouabain. Initially, cells are bathed in a medium containing fluorescent dye at temperatures prohibitive to endocytosis. The bath is quickly warmed to let endocytosis begin. The total integrated fluorescence of the dye taken up by the newly formed endosomes is measured, and the acidification curves are determined. These acidification curves are averaged recordings from the entire endosomal population as it undergoes all stages of endocytosis. The early measurements are presumably dominated by those endosomes undergoing early endocytosis, and it is in this early portion in which the effects of ouabain are particularly acute.

In Fig. 7, we modeled the initial acidification of the entire endosomal population with a single average spherical vesicle. All simulations included buffering capacity, chloride and potassium channels, V-ATPases, and proton leak. The initial pH of the vesicle was that of the bathing solution, and all internal ion concentrations were assigned standard extracellular values from Table I. The middle dashed curve is the simulation in the presence of Na,K-ATPases, whereas the bottom curve is the same simulation in the absence of Na,K-ATPases. We sought a single set of parameters that could simulate the dynamics of acidification both in the presence (Fig. 7, circles) and absence of ouabain (Fig. 7, diamonds) simply by turning off the Na,K-ATPase. From the two lower curves, we see that our model could not fit both sets of data with this constraint. In the presence of chloride and potassium counter ion conductance, it is very difficult for the Na,K-ATPase to increase the membrane potential enough to limit acidification by more than half a pH unit.

From our studies, the Na,K-ATPase is able to limit acidification by a whole pH unit only (1) when the endomembrane no longer conducts chloride above a certain critical membrane potential, or (2) when the initial internal potassium concentration is far greater than typical external values and there is no chloride conductance. To explore the former hypothesis, we replaced the passive chloride channel, described by Eq. 2, with a voltage-gated channel that has zero conductance when
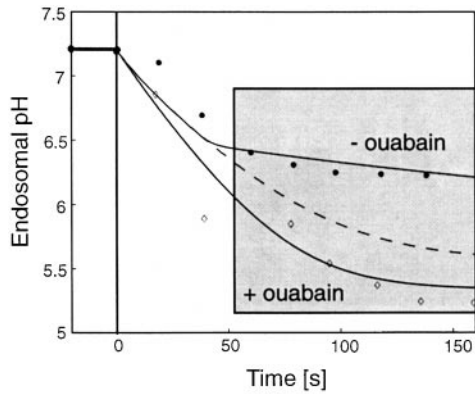
FIGURE 7. Endosomal acidification in the selective presence ($-$ ouabain) or absence ($+$ ouabain) of Na,K-ATPase. We model the acidification of a single 163-nm-diam spherical endosome in the presence (top curves) or absence (bottom curves) of 350 Na,K-ATPases. All three simulations include the following: 16 V-ATPases, a proton leak with a permeability of 8.24×10^{-5} cm/s, chloride channels, passive potassium channels, 140 mM of Donnan particles, and 40 mM/(pH unit) buffering capacity. The initial lumenal concentrations of sodium and potassium were assumed equal to standard extracellular values (Table I). A significant increase in lumenal pH is achieved by incorporating Na,K-ATPases into the vesicle (dashed curve). However, the addition of a voltage-gated chloride channel, which is inactivated above 133 mV, is necessary to obtain the experimentally measured full pH difference (top curve). Data points have been adapted from Cain et al. (1989). The model endosome begins acidifying at a single instance, hence, a kink in the pH is present at time zero. The experimental points are smoother since only a small fraction of the what will be the entire endosomal population has begun acidifying near time zero. We have shaded the graph at later times to highlight the portion of the curves best modeled by a single endosome.

the total membrane potential exceeds 83 mV. In the presence of such a voltage-gated chloride channel, the middle dashed line becomes the top solid curve (Fig. 7), whereas the simulation in the absence of Na,K-ATPases remains unchanged from the bottom curve. Without Na,K-ATPases, the steady-state membrane potential is below the switching voltage of the activated chloride channels, and the chloride counter ions mask the movement of protons into the lumen. The addition of Na,K-ATPases pushes the membrane potential above the switching voltage of the chloride channel, and the chloride ions no longer act as counter ions. As the pumps continue to push protons into the lumen, the membrane potential quickly increases. This adversely affects the V-ATPase pumping rate resulting in a much more alkaline lumen.

From the two solid curves in Fig. 7, we see that the presence of a voltage-gated chloride channel, first proposed in this context by Rybak et al. (1997), greatly increases the ability of the Na,K-ATPase to affect lumenal pH. ClC-5 is a chloride channel that localizes to endosomes in proximal tubule cells; it is a likely candidate for the chloride conductance in the experiments exam-

ined here (Günther et al., 1998). This protein belongs to the ClC family of chloride channels that exhibit widely varying current-voltage dependencies (Maduke et al., 2000). For inside positive voltages, ClC-5 channels carry a small inward flux of chloride; however, this flux does not vanish for total membrane potentials >83 mV as we hypothesize above (Friedrick et al., 1999). Without such a gated chloride channel, or the presence of a high initial potassium concentration in the endosome coupled with no chloride conductance, our model predicts that the Na,K-ATPase can alkalinize the lumen by half of a pH unit, at most.

Lumenal pH Is Most Sensitive to Changes in Pump and Leak Densities

We have reviewed many experiments that attempt to address the importance of particular regulatory elements in establishing and maintaining pH. Our model includes many of these elements, and it is important to determine the relative sensitivity of each of these regulatory factors. In principle, such analysis will help experimenters determine which parameters are most critical to the type of questions they want to answer. We chose to revisit the Golgi complex simulations in Fig. 6 to carry out this sensitivity analysis.

The acidification of a model organelle was simulated from an initial lumenal pH of 7.4 until steady state was reached. All relevant parameters were varied $\pm10\%$ from the original values given in Table IV. As in Fig. 5, the proton pump and leak densities remain constant when the surface area is changed. The difference between the curves generated with and without variation were characterized in two ways: (1) the percentage change in the total pH gradient across the membrane ($\%\Delta pH$), and (2) the percent change in the half-time to acidification ($\%\tau$). The list of varied parameters is given in Table V, along with the values for $\%\Delta pH$ and $\%\tau$.

From the top two entries in Table V, we see that the most effective ways to change the steady-state pH are to vary the density of active proton pumps or proton leaks

Sensitivity Analysis

Parameter	Percent change ΔpH	Percent change τ
H$^+$ permeability	−7.5/8.3	−0.2/0.4
Number of V-ATPases	7.5/−8.3	−8.8/10.9
Cytoplasmic potassium	−3.5/3.9	1.4/−1.5
Donnan particles	3.4/−3.6	−1.2/1.3
Cytoplasmic surface potential	1.5/−1.4	−4.2/5.1
Cytoplasmic chloride	0.5/−0.5	−0.2/0.2
Buffering capacity	−0.3/0.3	10/−10
Volume	0.0/0.0	10/−10
Surface area	0.0/0.0	−9.0/11

Sensitivity analysis of lumenal pH and time to acidification. The parameter values describing the acidification of the Golgi complex (Table IV) have been individually varied ±10%, and the resulting percent change in the lumenal pH gradient and time constant are given. Percentages on the left side of the slash correspond to the positive variation in the parameter. Experimental quantities are listed in order of decreasing influence on steady-state pH. The external potassium and chloride concentrations were 140 and 20 mM, respectively.

(permeability). Thus, the principle determinant of the steady-state Golgi complex pH is the ratio of the proton pump rate to the proton leak rate. The Donnan particles, surface potential, and external potassium concentration influence the pH gradient indirectly by altering the membrane potential, as discussed in the analysis of Fig. 4 (C and D). The chloride concentration acts in a similar manner, but with a smaller effect due to reduced changes in concentration. The pH gradient is least sensitive to the last three parameters: buffering capacity, volume, and surface area. However, these elements dramatically influence the transient pH dynamics. Thus, the relative importance of a particular regulatory element to an experiment depends on whether transient or steady-state measurements are being made. For instance, experiments that attempt to determine the proton permeability of a specific organelle, as in Fig. 6, require accurate knowledge of the volume, surface area, and buffering capacity to meaningfully model the transient data.

It is important to realize that this sensitivity analysis pertains to the acidification of the Golgi complex. Many of the trends in Table V will persist for descriptions of different organelles; however, the values will surely be different. For example, changes in the volume of endosomes had no noticeable effect on the acidification curve, yet comparable percent changes in the Golgi complex volume are quite noticeable. In addition, this analysis is only valid for determining the relative importance of each parameter near the target pH of the Golgi complex.

Sensitivity analysis confirms what has been a general theme throughout this paper: steady-state pH is most dependent upon proton pump and leak densities. However, transient data is most sensitive to volume, surface area, buffering capacity, and proton pump density.

The model provides a method to explore different mechanisms in comparison with experimental data focusing on the most sensitive parameters.

DISCUSSION

We have constructed a quantitative model for organelle acidification that can be tailored to address many of the organelles along the secretory and endosomal pathways. Thus, the model can provide a general framework for understanding acidification. By using physically accurate descriptions of but a handful of pH regulatory elements, we have been able to successfully model the acidification of several organelles. The close attention paid to the biochemical makeup of the systems studied eliminated some of the extreme pH and membrane potential values predicted in the earlier work of Rybak et al. (1997). We have presented the first estimates of Golgi complex proton permeability, ∼10^{-5} cm/s, as well as the first predictions of the active ATPase pump numbers for the Golgi complex and endosome. By modeling experimental data, we were able to make hypotheses about the regulatory elements present in specific organelles. Our model suggests that the Golgi complex is permeable to at least two dominant counter ions. In the endosome, we conclude that it is possible for the Na,K-ATPase to limit lumenal acidification by increasing the membrane potential. However, the presence of voltage-gated chloride channels or extreme ionic conditions are required to explain the high degree with which the Na,K-ATPase has been shown to limit acidification.

The greatest asset of our model lies in its ability to quantify and compare experimental data; however, a good deal of our analysis has been spent justifying the accuracy of our approach. We have not addressed what biochemical differences are required to elicit pH changes between organelles. Secretory granules that bud from the Golgi complex at pH ≈ 6.4 eventually achieve lumenal pHs of ∼5.4. Table V suggests that changes in the proton pump and leak density are most effective in bringing about this 1-pH unit drop. Calculations were performed on a 200-nm-diam vesicle with properties similar to the Golgi complex simulation of Fig. 6. A 10-fold increase in the proton pump density or a 10-fold decrease in the proton permeability proved sufficient to describe this drop in lumenal pH. Ultimately, we hope that analyses such as these, in conjunction with experimental data, will help elucidate the nature of pH regulation in the cell.

It is interesting to note the discrepancy in proton permeabilities between reconstitution and intact cell experiments. Proton permeability values deduced from reconstitution experiments are ∼100 times higher than values deduced from data recorded from intact cells. It is possible that the process of reconstitution artificially increases the proton permeability of the membrane.

Extending the model to describe additional organelles can be accomplished easily by including the specialized proteins that make these systems unique; e.g., synaptic vesicles that use the proton gradient to drive the uptake of neurotransmitter. This is the approach we used in modeling the early-to-late endosome transition, which required a detailed model of the Na,K-ATPase. Some of the most acidic organelles, such as lysosomes and the central vacuoles of plant cells, have not been discussed. Lemon vacuoles have been shown to acidify to pH 2.5, whereas giant blood cells of the marine *Ascidian* have single large vacuoles with lumenal pHs below 1 (Muller et al., 1996; Futai et al., 1998). It is not clear how the V-ATPase could be solely responsible for creating such acidic environments since it is generally thought to be thermodynamically limited to a maximum pH difference of 4.5 units. It is possible that another enzyme contributes to acidification of these systems or that other regulatory elements conspire to create a very negative membrane potential that helps to drive protons into the lumen. Motivated by the presence of V-ATPases in lemon vacuoles, we previously proposed a mechanism by which the V-ATPase proton pump could "change gears" and pump below pH 1 (Grabe et al., 2000). In *Online Supplemental Material* (see http://www.jgp.org/cgi/content/full/117/4/329/DC1), we describe the molecular mechanism of this gear change and include a calculation confirming that this hypothetical scheme can indeed produce large pH gradients.

REFERENCES

Alberts, B., D. Bray, J. Lewis, M. Raff, K. Roberts, and J. Watson. 1994. Molecular Biology of the Cell. 3rd ed. Garland Press, New York, NY. 1294 pp.

Belcher, J.D., R.L. Hamilton, S.E. Brady, C.A. Hornick, S. Jaeckle, W.J. Schneider, and R.J. Havel. 1987. Isolation and characterization of three endosomal fractions from the liver of estradiol-treated rats. *Proc. Natl. Acad. Sci. USA.* 84:6785–6789.

Cahalan, M.D., and J.E. Hall. 1982. Alamethicin channels incorporated into frog node of ranvier: calcium-induced inactivation and membrane surface charges. *J. Gen. Physiol.* 79:411–436

Cain, C.C., D.M. Sipe, and R.F. Murphy. 1989. Regulation of endocytic pH by the Na⁺,K⁺-ATPase in living cells. *Proc. Natl. Acad. Sci. USA.* 86:544–548.

Chatterjee, D., M. Chakraborty, M. Leit, L. Neff, S. Jamsa-Kellokumpu, R. Fuchs, M. Bartkiewicz, N. Hernando, and R. Baron. 1992. The osteoclast proton pump differs in its pharmacology and catalytic subunits from other vacuolar proton ATPases. *J. Exp. Biol.* 172:193–204.

DeCoursey, T.E., and V.V. Cherny. 2000. Common themes and problems of bioenergetics and voltage-gated proton channels. *Biochim. Biophys. Acta.* 1458:104–119.

Endresen, L.P., K. Hall, J.S. Hoye, and J. Myrheim. 2000. A theory for the membrane potential of living cells. *Eur. Biophys. J.* 29:90–103.

Farinas, J., and A.S. Verkman. 1999. Receptor-mediated targeting of fluorescent probes in living cells. *J. Biol. Chem.* 274:7603–7606.

Friedrick, T., T. Breiderhoff, T. Jentsch. 1999. Mutational analysis demonstrates that ClC-4 and ClC-5 directly mediate plasma membrane currents. *J. Biol. Chem.* 274: 896–902

Fuchs, R., S. Schmid, and I. Mellman. 1989. A possible role for sodium, potassium-ATPase in regulating ATP-dependent endosome acidification. *Proc. Natl. Acad. Sci. USA.* 86:539–543.

Futai, M., T. Oka, Y. Moriyama, and Y. Wada. 1998. Diverse roles of single membrane organelles: factors establishing the acid lumenal pH. *J. Biochem.* 124:259–267.

Futai, M., T. Oka, G.-H. Sun-Wada, Y. Moriyama, H. Kanazawa, and Y. Wada. 2000. Luminal acidification of diverse organelles by V-ATPase in animal cells. *J. Exp. Biol.* 203:107–116.

Grabe, M., H. Wang, and G. Oster. 2000. The mechanochemistry of V-ATPase proton pumps. *Biophys. J.* 78:2798–2813.

Günther, W., A. Luechow, F. Cluzeaud, A. Vandewalle, T. Jentsch. 1998. ClC-5, the chloride channel mutated in Dent's disease, colocalizes with the proton pump in endocytotically active kidney cells. *Proc. Natl. Acad. Sci. USA.* 95:8075–8080.

Hartmann, T., and A.S. Verkman. 1990. Model of ion transport regulation in chloride-secreting airway epithelial cells. Integrated description of electrical, chemical, and fluorescence measurements. *Biophys. J.* 58:391–401.

Heyse, S., I. Wuddel, H.-J. Apell, and W. Stuermer. 1994. Partial reactions of the Na,K-ATPase: determination of rate constants. *J. Gen. Physiol.* 104:197–240.

Hill, W.G., R.L. Rivers, and M.L. Zeidel. 1999. Role of leaflet asymmetry in the permeability of model membranes to protons, solutes, and gases. *J. Gen. Physiol.* 114:405–414.

Hille, B. 1992. Ionic Channels of Excitable Membranes. 2nd ed. Sinauer Associates, Inc., Sunderland, MA. 607 pp.

Hodgkin, A.L., and A.F. Huxley. 1952. A quantitative description of membrane current and its application to conduction and excitation in nerve. *J. Physiol.* 117:500–544.

Israelachvili, J.N. 1992. Intermolecular and Surface Forces. 2nd ed. Academic Press Inc., London. 450 pp.

Kim, J.H., C.A. Lingwood, D.B. Williams, W. Furuya, M.F. Manolson, and S. Grinstein. 1996. Dynamic measurement of the pH of the Golgi complex in living cells using retrograde transport of the verotoxin receptor. *J. Cell Biol.* 134:1387–1399.

Ladinsky, M.S., D.N. Mastronarde, J.R. McIntosh, K.E. Howell, and L.A. Staehelin. 1999. Golgi structure in three dimensions: functional insights from the normal rat kidney cell. *J. Cell Biol.* 144: 1135–1149.

Lauger, P., and H.-J. Apell. 1986. A microscopic model for the current-voltage behaviour of the Na,K-pump. *Eur. Biophys. J.* 13:309–321.

Lencer, W.I., P. Weyer, A.S. Verkman, D.A. Ausiello, and D. Brown. 1990. FITC-dextran as a probe for endosome function and localization in kidney. *Am. J. Physiol.* 258:C309–C317.

Maduke, M., C. Miller, and J. Mindell. 2000. A decade of CLC chloride channels: structure, mechanism, and many unsettled questions. *Annu. Rev. Biophys. Biomol. Struct.* 29:411–438

McLaughlin, S. 1989. The electrostatic properties of membranes. *Annu. Rev. Biophys. Biophys. Chem.* 18:113–136.

McLaughlin, S., N. Mulrine, T. Gresalfi, G. Vaio, and A. McLaughlin. 1981. Adsorption of divalent cations to bilayer membranes

containing phosphatidylserine. *J. Gen. Physiol.* 77:445–473.

Moriyama, Y., and M. Futai. 1990. Proton-ATPase, a primary pump for accumulation of neurotransmitters, is a major constituent of brain synaptic vesicles. *Biochem. Biophys. Res. Comm.* 173:443–448.

Moriyama, Y., M. Maeda, and M. Futai. 1992. Involvement of a non-proton pump factor (possibly Donnan-type equilibrium) in maintenance of an acidic pH in lysosomes. *FEBS Lett.* 302:18–20.

Muller, M., U. Irkens-Kiesecker, B. Rubinstein, and L. Taiz. 1996. On the mechanism of hyperacidification in lemon. *J. Biol. Chem.* 271:1916–1924.

Paula, S., A.G. Volkov, A.N. Van Hoek, T.H. Haines, and D.W. Deamer. 1996. Permeation of protons, potassium ions, and small polar molecules through phospholipid bilayers as a function of membrane thickness. *Biophys. J.* 70:339–348.

Press, W.H. 1997. Numerical Recipes in C: The Art of Scientific Computing. 2nd ed. Cambridge University Press, New York, NY. 994 pp.

Roos, A., and W.F. Boron. 1981. Intracellular pH. *Physiol. Rev.* 61: 296–434.

Rothman, J.E., and J. Lenard. 1977. Membrane asymmetry. *Science.* 195:743–753.

Rybak, S., F. Lanni, and R. Murphy. 1997. Theoretical considerations on the role of membrane potential in the regulation of endosomal pH. *Biophys. J.* 73:674–687.

Sagar, A., and R.F. Rakowski. 1994. Access channel model for the voltage dependence of the forward-running Na$^+$/K$^+$ pump. *J. Gen. Physiol.* 103:869–894.

Schapiro, F., and S. Grinstein. 2000. Determinants of the pH of the Golgi complex. *J. Biol. Chem.* 275:21025–21032.

Shi, L., K. Fushimi, H. Bae, and A.S. Verkman. 1991. Heterogeneity on ATP-dependent acidification in endocytic vesicles from kidney proximal tubule. *Biophys. J.* 59:1208–1217.

Sokolov, V.S., H.-J. Apell, J.E.T. Corrie, and D.R. Trentham. 1998. Fast transient currents in Na,K-ATPase induced by ATP concentration jumps from the P3-(1-(3′,5′-dimethoxyphenyl)-2-phenyl-2-oxo)ethyl ester of ATP. *Biophys. J.* 74:2285–2298.

Teter, K., G. Chandy, B. Quinones, K. Pereyra, T. Machen, and H.-P. Moore. 1998. Cellubrevin-targeted fluorescence uncovers heterogeneity in the recycling endosomes. *J. Biol. Chem.* 273:19625–19633.

Van Dyke, R.W. 1993. Acidification of rat liver lysosomes: quantitation and comparison with endosomes. *Am. J. Physiol.* 265:C901–C917.

Van Dyke, R.W., and J.D. Belcher. 1994. Acidification of three types of liver endocytic vesicles: similarities and differences. *Am. J. Physiol.* 266:C81–C94.

Vander, A.J., J.H. Sherman, and D.S. Luciano. 1985. Human Physiology: The Mechanisms of Body Function. 4th ed. McGraw-Hill Inc., New York. 715 pp.

Verdugo, P. 1991. Mucin exocytosis. *Am. Rev. Respir. Dis.* 144:533–537.

Weiss, T.F. 1996. Cellular Biophysics. MIT Press, Cambridge, MA. 693 pp.

Wu, M., J. Llopis, S. Adams, J. McCaffery, T. Machen, H.P. Moore, and R. Tsien. 2000. Using targeted avidin and membrane permeant fluorescent biotin to study secretory pathway organelle pH regulation. *Chem. Biol.* 7:197–209.